Kinetics of hydrogenation of acetic acid over supported platinum catalyst

Lawal, Ahmed; Hart, Abarasi; Daly, Helen; Hardacre, Christopher; Wood, Joe

DOI:
10.1021/acs.energyfuels.9b01062

Document Version
Peer reviewed version

Citation for published version (Harvard):
Lawal, A, Hart, A, Daly, H, Hardacre, C & Wood, J 2019, 'Kinetics of hydrogenation of acetic acid over supported platinum catalyst', *Energy & Fuels*, vol. 33, no. 6, pp. 5551-5560.
https://doi.org/10.1021/acs.energyfuels.9b01062

Kinetics of hydrogenation of acetic acid over supported platinum catalyst

Ahmed M. Lawal[1], Abarasi Hart[1], Helen Daly[2], Christopher Hardacre[2] and Joseph Wood[1]*

[1]School of Chemical Engineering, University of Birmingham, Edgbaston, Birmingham, B15 2TT, UK

[2]School of Chemical Engineering and Analytical Science, University of Manchester, M13 9PL, UK

Keywords: Hydrogenation, Bio-oil, acetic acid, kinetics

ABSTRACT: Petroleum is non-renewable and contributes to environmental pollution, thus bio-oil can be substituted as a potential alternative. However, bio-oil in its crude form cannot be used directly as fuel since it contains high proportion of oxygenated, acidic and reactive compounds such as carboxylic acids. These are known to cause corrosion of vessels and pipework, instability and phase separation. The heating value of bio-oil can be improved through hydrodeoxygenation (HDO). In this study, HDO of acetic acid is presented, being a typical model compound found in bio-oil. Kinetic data were obtained over the range of temperature: 175 - 210 ºC, hydrogen pressure: 20-50 bar, initial acetic acid concentration: 0.16-0.521 M and catalyst loading: 0.2-0.5 g, in a 100mL batch reactor using 4% Pt/TiO_2. It was found that catalyst particle sizes < 65 μm and a stirring speed of 1000 min^{-1} were sufficient to overcome internal and external mass transfer

resistances and ensure that the reaction is within the kinetic regime. A Langmuir-Hinshelwood model, assuming competitive adsorption of dissociative H_2 and acetic acid, fitted the experimental data.

1. INTRODUCTION

Petroleum-based transportation fuels account for most of the world transportation energy consumption which increases at an annual average rate of 1.4%, and this growth is expected to continue through to 2040.[1] In order to cut down the emissions from the combustion of petroleum fuels for transportation, bio-oil, which is a renewable carbon-based fuel, has shown potential for production of valuable chemicals and transportation fuels.[2] However, it is a complex mixture of oxygenated compounds produced from pyrolysis of biomass such as wood. Despite its merits, bio-oil has been characterized by acidity, high viscosity, high oxygen content and chemical instability, which adversely affects its heating value.[3] Upgrading has become a necessity to improve the fuel properties but the complexity of bio-oil makes it challenging to understand the upgrading chemistry and reaction pathways. The essence of upgrading therefore is to obtain a product with characteristics similar, equivalent or more sustainable compared to declining fossil fuels.

Hydrodeoxygenation (HDO) has been considered as one of the processes for upgrading bio-oil. However, the process has suffered from issues associated with catalyst deactivation, uneconomical process cost and poor understanding of the kinetics.[2,3] HDO involves the conversion or removal of oxygenates in the bio-oil in the presence of suitable catalyst, hydrogen pressure and temperature to produce hydrocarbon products. It is therefore crucial to develop a more efficient heterogeneous catalyst which is less susceptible to deactivation.

Generally, bio-oil is composed of approximately 15% carboxylic acid, mainly acetic and formic acids.[4,5] This makes it highly acidic in nature, with a pH range of 2.8-3.8, and has the potential to

sufficiently catalyse reactions. This results in continuous degradation and alteration of bio-oil properties. Studies on hydrogenation of carboxylic acids have mainly focused on high molecular weight acids such as fatty acids with less emphasis on low molecular weight acids. Bio-oils generally contain a large water content (typically 15-30%).[6,7] Therefore, most studies have been focused on the processing of this aqueous phase.

The catalytic HDO of carboxylic acids to their corresponding alcohols and other valuable hydrocarbons is an effective route for bio-oil utilization. The generation of these products depends on the type of catalyst and reaction mechanism. Hydrogenolysis and ketonization are the predominant pathways that describe the generation of alcohols and other products such as esters. In contrast to the hydrogenation of amides[8,9] and esters[10,11] which are straightforward and effective synthetic methods to generate alcohols and other fine chemicals, carboxylic acids are difficult to hydrogenate. Due to the low electrophilicity of carbonyl carbon and its interaction with the catalyst,[12–14] this results in thermodynamic and kinetic stability of the carboxylic acids. In continued efforts to address these challenges, several studies have been performed using heterogeneous and homogenous catalysts, yielding commercial viability for some processes. However, the reaction requires harsh operating conditions in the range of 200-300 °C and hydrogen pressure of 140-300 bar, thereby favouring side reactions and degradation of reaction substrates,[15] and a low yield of targeted products may be achieved. Hydrogenation of long chain carboxylic acids using heterogeneous catalysts have mainly proceeded via hydrogenation-dehydration-hydrogenation reaction pathway to yield alcohols and alkanes. For example, Manyar et al.[16] have studied the hydrogenation of fatty acids using titania supported Pt catalysts to generate alcohols and alkanes. Similarly, Ullrich and Breit[17] reported the same reaction pathway for the hydrogenation of long chain carboxylic acids using Pd-Re/C. On the other hand, Zhou et al.[18]

investigated the kinetic modelling of acetic acid over modified Pt-Sn/Al_2O_3 in a fixed bed reactor at 350 °C. Similarly, Rachmady and Vannice[19] studied the kinetic modelling of acetic acid over Pt/TiO_2 at 150-300 °C. These studies only considered a model that incorporates dissociative adsorption of hydrogen and acetic acid. Wan et al.[20] investigated the role of different noble metal catalysts over different supports and revealed that Ru/C had the highest activity but favoured gaseous products. Chen et al.[21] studied the HDO of different organic acids and their mixtures, and have reported the kinetics of the system taking into account competitive adsorption of reactants and product inhibition. From various studies on hydrogenation of carboxylic acids, the mechanism that favors production of alcohols and alkanes on further hydrogenation appears to be more generic for long chain acids.

Since most reported studies are mainly on long chain carboxylic acids components of the bio-oil, this study will focus on acetic acid. The role of process parameters such as pressure, temperature an catalyst loading on the reaction mechanism for HDO of acetic acid over prepared 4% Pt/TiO_2 catalyst are examined using a batch reactor system. The reaction mechanism and kinetic modelling were studied by fitting a Langmuir-Hinshelwood expression to the experimental data. The choice of 4% Pt/TiO_2 catalyst for this study was established from catalyst screening in our previous study.[22]

2. EXPERIMENTAL SECTION

2.1. Materials. Acetic acid with 99.5% purity was purchased from Sigma Aldrich. Ethanol (purity 99%), hexane (HPLC grade, 95%) and ethylacetate (99%) both purchased from Fisher scientific, UK. Platinum (IV) nitrate, and methanol (purity 99%) were acquired from Alfa Aesar

and titanium dioxide (P90) was obtained from Evonik industries, UK required for the catalyst preparation.

2.1. Catalyst Preparation. 4% Pt/TiO_2 was prepared by incipient wetness impregnation method using titanium dioxide (P90) as support and platinum (IV) nitrate [Pt $(NO_3)_4$ (15% w/w)] as the metal precursor. 2.93 g of platinum nitrate was added dropwise to 9.6 g of titanium dioxide (P90) to make up 10g of 4% Pt/TiO_2. A suspension solution was formed by adding 100 ml of methanol to the resulting mixture which was stirred overnight using a magnetic stirrer at room temperature. The resulting suspension was filtered and the paste residue was oven dried for 3 hours at a temperature of 80 °C. After oven drying, the solid was ground into powder form using pestle and mortar, and calcined at 500 °C under air flow for 4 hours.

2.2. Catalyst Characterization. A scanning electron microscope (SEM Hitachi TM3030 Plus) with accelerating voltage of 15 keV was used to study the surface morphology of the catalyst. The dispersion of active metals and elemental composition was validated by Energy Dispersive X-ray spectroscopy (EDX) which is equipped with the SEM. The Brunauer–Emmett–Teller (BET) microstructural properties were evaluated by nitrogen adsorption and desorption on the catalyst surface at 77 K, using a micrometrics analytical instrument ASAP 2010. X-Ray diffraction (XRD) patterns were measured using a D2 Bruker diffractometer and Cu Kα radiation to obtain the different crystal phases.

2.3. Experimental Procedure. Hydrogenation reactions were carried out using a 100 ml stirred autoclave reactor (Parr Instruments Company, USA), equipped with a mechanical stirrer, thermocouple, pressure gauge and a control system for temperature. The reactor is equipped with a bursting disk, inlet and outlet gas ports and a retrofitted liquid sampling port. The reactions were performed in a temperature range of 175-210 °C at different hydrogen pressures (20-50 bar) and

catalyst loadings (0.2-0.4 g) with conditions shown in Table 1. Prior to reactions, 0.3 g of 4% Pt/TiO_2 catalyst was typically added to 50 mL of hexane inside the reactor and reduced in-situ at a temperature of 200 °C under a stirring speed of 1000 min^{-1} and hydrogen pressure of 20 bar for 65 minutes. Subsequently, a desired amount of acetic acid was added into the reactor and sealed. The reactor was then purged with hydrogen gas and further pressurized to 50 bar, and allowed to stabilize for five minutes to ensure a leak-proof system. The reactor was heated up to the desired temperature typically in the range of 175-210 °C at a rate of 13 °C/min. Subsequently, the reaction was commenced by initiating a stirring speed of 1000 min^{-1}. Nine liquid samples (1 ml each) were collected per reaction at 40 minutes interval, followed by flushing of sample line with hexane after each sample collection. The composition of the reaction was considered unaffected by the collection of approximately 10 ml of sample during the reaction which accounts for 20% of the reaction mixture. At the end of the reaction after 6 hours, the reactor was cooled and depressurized.

Table 1. Experimental Conditions

Process variables	Value
Temperature (°C)	175-210
Hydrogen pressure (bar)	20-50
Catalyst loading (g)	0.2-0.4
Substrate concentration (M)	0.16-0.5
Agitation speed (min^{-1})	600-1400
Reaction time (h)	1-6

2.4. Analytical Technique. The reaction products were identified using a gas chromatography equipped with mass spectrometer (GC-MS Agilent 7890A). The amount of the acetic acid converted and the liquid products formed from the experiments were quantified using Shimadzu

GC-2010 equipped with flame ionization detector (FID) and 30 m × 0.25 mm × 0.25 μm ZB-Wax capillary column. Prior to the analysis, the samples were spiked with butanol as an internal standard in a ratio of 10:1. The GC was operated under a constant pressure mode with a split flow of 181. The injector and detector temperatures were set at 250 °C. To separate the products, the GC oven was held at 40 °C for 5 minutes and then subsequently heated to 215 °C at a ramp rate of 20 °C.min^{-1}. Further heating to 220 °C was carried out with a ramping of 5 °C.min^{-1} and held for 5 minutes. Injections were repeated three times and were reproducible with an error of < 2%. The following equations were used to quantify the acetic acid conversion and product selectivity.

$$\text{Conversion (\%)} = \frac{(\text{Initial moles of acid} - \text{Final moles of acid})}{\text{Initial moles of acid}} \times 100$$

$$\text{Selectivity (\%)} = \frac{\text{Moles of desired product}}{\text{Total moles of products formed}} \times 100$$

2. RESULTS AND DISCUSSION

3.1. Catalyst Characterization. Figure 1 shows the SEM micrograph of the prepared and used catalysts. The surface topography and morphology are distinct; for the fresh catalyst, the TiO_2 particulate sizes range from 1-2.5 μm with dispersed Pt grains. While after 4 h of reaction over fresh cycle and two reuse cycles as reported in our previous work,[22] the particles formed agglomerates in the range of 2-7μm. These changes can be linked to the surface reaction. It can be observed on the morphology of the used catalyst features of tiny holes which are absent in the fresh counterpart, which can be attributed to the loss of some impregnated Pt grains during reaction. EDX result also showed that platinum is well-dispersed on the catalyst surface (Figure S1).

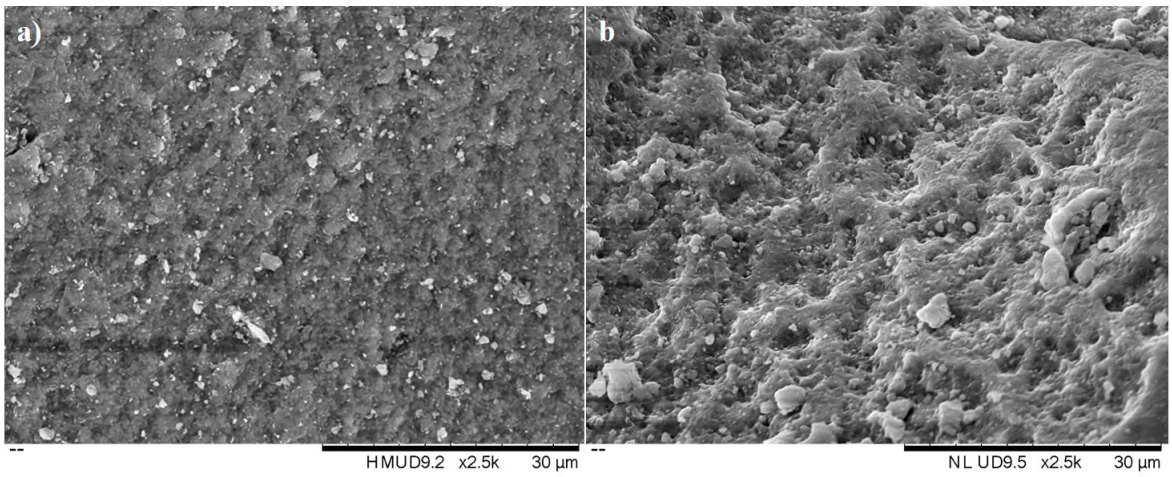

Figure 1. SEM images for a) fresh b) spent 4% Pt/TiO_2 catalyst.

The nitrogen-sorption isotherm for the surface area determination and pore structure is shown in Figure S2. The hysteresis loop of the adsorption and desorption curve shows a Type IV isotherm which represents a mesoporous material with pore size in the range of 2-50 nm.[23] It is also apparent that a limited amount of nitrogen physisorption occurs within the region of 0 to 0.5 relative pressure while the uptake of nitrogen increases with increasing relative pressure from 0.5 to 0.9. This corresponds to the occurrence of capillary condensation, and enables determination of pore size and pore volume.[24] The specific surface area of the fresh 4% Pt/TiO_2 is 97 $m^2.g^{-1}$, while that of the spent catalyst is 92 $m^2.g^{-1}$. In the same vein, the pore volume for the fresh and spent catalysts are 0.184 $cm^3.g^{-1}$ and 0.172 $cm^3.g^{-1}$ respectively. The observed decrease in surface area and pore volume for the spent catalyst can be associated to findings from SEM analysis which showed the formation of agglomerates due to loss of impregnated Pt grains and subsequent shrinkage of active sites.

The XRD pattern of 4% Pt/TiO_2 can be found in Figure S3. It is clear that TiO_2 and Pt/TiO_2 have the same pattern, and contain diffractions that can be attributed to the anatase and rutile phases of TiO_2.[25,26] The most distinct peak at $2\theta = 25^{o}$ and others at 38^{o}, 48^{o}, 55^{o} and 63^{o} corresponds to

miller indices (101), (004), (200), (211), and (002) diffractions of tetragonal TiO_2, respectively. The absence of peaks due to PtO absence indicates that Pt/TiO_2 has highly dispersed platinum particles (< 4 nm) .

3.2. Mass Transfer Considerations. Catalytic hydrogenation of acetic acid is a three-phase reaction involving hydrogen (gas), the reactant medium (liquid) and heterogeneous catalyst (solid). For a chemical reaction to occur, hydrogen has to diffuse from the gas phase into the bulk liquid phase through the gas-liquid boundary layer and subsequently onto the external surface of the catalyst. At the same time, acetic acid is transferred from the bulk liquid phase into the external surface of the catalyst before reaction can occur. Therefore, it is imperative to eliminate external and internal mass transfer limitation in order to ensure reaction rates were evaluated under kinetic control.

3.2.1. External Mass Transfer. During reactions involving identical temperature and hydrogen pressure, the rate of hydrogen mass transfer in the gas-liquid boundary is determined by k_La, and is mainly influenced by various factors such as the reactor impeller, internal diameter, speed of agitation and type of solid/liquid. For example, Zhang et al.[27] reported an increase in k_La from 0.005 s^{-1} to 0.09 s^{-1} as the stirring speed increases from 200 min^{-1} to 1200 min^{-1} during the hydrogenation of lactic acid over ruthenium on carbon catalyst. The extent of agitation speed for a given reaction system and reactor configuration appears to be significant towards the k_La value.[28,29] Therefore, a minimum stirring speed (N_m) required to ensure complete suspension of 4% Pt/TiO_2 catalyst particles for the present batch system was calculated using the Zwietering correlation and was found to be 588 min^{-1} (Table S1). Subsequently, a set of experiments were

carried out at varied stirring speeds in the range of 600 min^{-1} to 1400 min^{-1} (all above N_m = 588 min^{-1}) to investigate the effect of agitation on mass transfer rate.

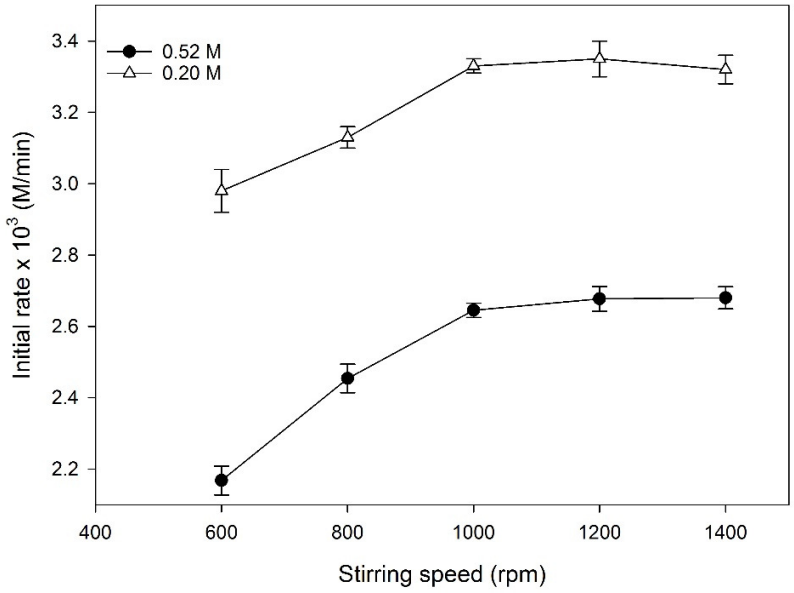

Figure 2. Effect of stirring speed on reaction rates (H_2 pressure, 40 bar; catalyst loading, 0.3 g; temperature, 200 °C and reaction time, 2 h, respectively).

Figure 2 shows the influence of stirring speed on rate of acetic acid hydrogenation at different initial concentrations. As seen in Figure 2, it is clear that the reaction rates were strongly dependant on stirring speed between 600-1000 min^{-1}, at which the rates increased from 0.0022±0.04 $M.min^{-1}$ to 0.0026±0.02 $M.min^{-1}$ and 0.0029±0.06 $M.min^{-1}$ to 0.0033±0.02 $M.min^{-1}$ for 0.52M and 0.20M respectively. The observed low reaction rates between 600 to 800 min^{-1} indicates the occurrence of gas-liquid mass transfer limitation since the lowest stirring speed of 600 min^{-1} investigated was greater than the calculated minimum speed (N_m = 588 min^{-1}) to ascertain uniform dispersion of the catalyst particles. At stirring speed exceeding 1000 min^{-1}, it was observed that the reaction rates

were invariant within experimental error. Therefore, the system was considered free from gas-liquid mass transfer regime at a minimum stirring speed of 1000 min^{-1}.

$$\frac{C_i}{R_A} = \frac{1}{k_{GL}a_B} + \frac{1}{w}\left(\frac{1}{k_{SL}a_P} + \frac{1}{k\eta}\right) \quad (1)$$

Given:

$\frac{1}{k_{GL}a_B}$ = resistance to gas adsorption

$\frac{1}{k_{SL}a_P} + \frac{1}{k\eta}$ = resistance to liquid-solid mass transfer and internal diffusion with surface reaction.

Mass transfer resistances across the gas-liquid boundary ($1/k_{GL}a_b$) and solid-liquid boundary ($1/k_{SL}a$) at 1000 min^{-1} were estimated experimentally using equation 1 and presented in Table 2.[30] It is worth noting that equation 1 is only valid for reactions with first order reaction kinetics. For non-first order reaction kinetics, the fitted parameters from equation 1 can be assumed to be an approximate estimation of the presence or absence of mass transfer limitations, but not for scale-up calculations.

Figure 3 shows a plot of the ratio of hydrogen concentration to reaction rate against the inverse of catalyst mass density in a range of 4 – 8 $dm^{-3}.g$. The intercept of the plot represents $1/k_{GL}a_b$, which is the resistance due to gas absorption across the gas-liquid interface and passes through the origin. On the other hand, the slope of the plot $1/k_{SL}a_p + 1/k$ represents the resistance of the solid-liquid interface and surface reaction, and was found to be 499.8 $dm^3.g^{-1}$. Since the gas-liquid mass transfer resistance passes through the origin, it suggests that the mass transfer effect across the gas-liquid interface in the present autoclave system was insignificant. Therefore, a stirring speed of 1000 min^{-1} was used in further hydrogenation experiments.

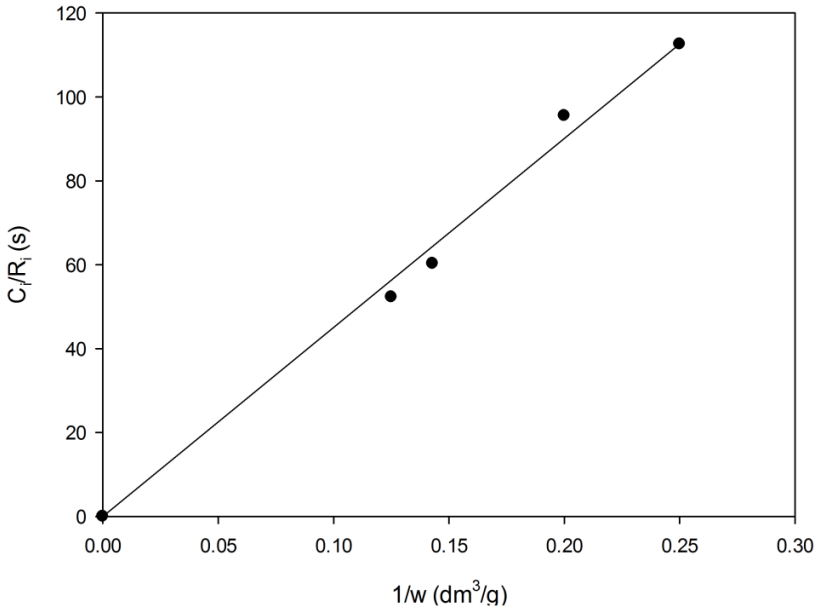

Figure 3. Mass transfer resistances for hydrogen across Gas-Liquid and Solid-Liquid boundaries (reaction conditions: initial concentration, 0.23 M; Stirring speed, 1000 min^{-1}; H_2 pressure, 40 bar; temperature, 200 °C and reaction time, 2 h respectively).

3.2.2. Internal Mass Transfer. The presence of catalytically active sites confined in the pores of spherical catalyst particles provides the platform for adsorption and reaction to occur. During reactions, the extent of hydrogen and acetic acid diffusion inside the pore network plays a significant role on the rate of reaction which necessitates the investigation of intra particle diffusional resistance. It has been reported in several studies,[31,32] that the significance of internal diffusion can be evaluated by investigating the particle size influence on reaction rates. Hence, the prepared 4% Pt/TiO_2 was sieved into the following particle size ranges < 63, 63-106, 106-160 and 160-250 μm and used for experiment under the same reaction conditions. Figure 4 shows the conversion of acetic acid and selectivity toward ethanol and ethylacetate as a function of catalyst particle size. While the selectivity of ethanol and ethylacetate are 23.2 and 76.8, respectively,

within observed experimental error for the different catalyst size range tested, the conversion of acetic acid narrowly decreases as the catalyst size increases. It can be concluded that the range of catalyst particle sizes investigated show a marginal variation on the hydrogenation activity, thus confirming that pore diffusion limitation can be neglected using the smallest particle size.[33,34] Therefore, the catalyst with particle size less than 63 μm was chosen for this study because a smaller particle size allows rapid diffusion of reactant and product molecules in and out of the catalyst, since the diffusion path length has been shortened, exposure to active sites enhanced and kinetic control rate enhanced.[35] Since both inter particle mass transfer and intra particle diffusional resistances have been eliminated under experimental conditions such as agitation speed of 1000 min^{-1} and catalyst particle size ≤63 μm, the reactions are considered to be performed in a kinetically controlled regime. Table 2 displays the values of the mass transfer and kinetics parameters obtained.

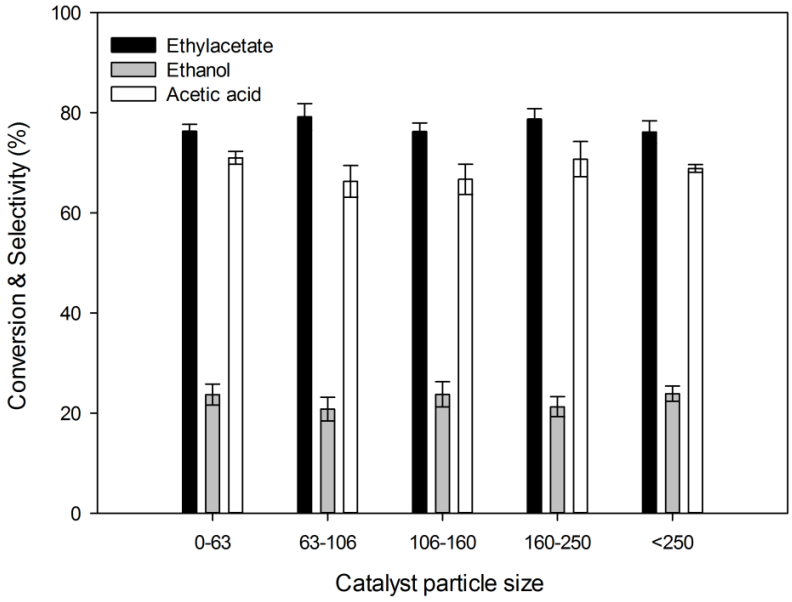

Figure 4. Investigation of internal diffusion using different catalyst particle size (reaction conditions: initial concentration, 0.521 M; H2 pressure, 40 bar; catalyst loading, 0.3 g; temperature, 200 °C; stirring speed, 1000 min^{-1} and reaction time, 2 h, respectively).

The absence of intra-particle diffusion was further validated by using the Weisz-Prater criterion (Equation 2).[29,36] This criterion utilizes the catalyst geometry and verifies the absence of internal diffusion if the measured value is less than 0.3 for reaction orders of ≤ 2.[35]

$$\eta\varphi^2 = \frac{r\omega L^2}{C_i D_{e_i}} \qquad (2)$$

where r is the initial rate, ω is the catalyst loading, L is the characteristic length of spherical particle, C_i is the reactant concentration and D_{ei} is the effective diffusivity. The particle characteristic length and reactants effective diffusivities (D_{ei}) were estimated using $L = \frac{D_p}{6}$ and Wilke-Chang correlations respectively.[37,38,39] The observable modulus $\eta\varphi^2$, which is the ratio of the reaction rate to the effective diffusion inside the catalyst pores, was found to be much less than 0.3 for both hydrogen and acetic acid (Table 2). Therefore, the rate of diffusion within the catalyst pore is greater than the reaction rate; hence, the influence of intra-particle diffusion can be neglected, as the reaction is found to be surface rate limited. Because equilibrium exists between dissolved hydrogen and hydrogen pressure, the concentration of dissolved hydrogen in hexane solvent was estimated by using the Henry's Law correlation as reported by Katayama and Nitta.[40]

$$C = kP_{H_2} \qquad (3)$$

Where P_{H_2} and k depend on the solubility of H_2 at a given temperature as given by Brunner.[40,41]

Table 2. Values of Weisz-Prater Modulus and parameters used to verify the absence of intra particle diffusion

ω ($Kg.m^{-3}$)	6
C_{acetic} (mM)	312
C_{H_2} (mM)	0.75
r $\times 10^4$ (kmol/(kgcat.min))	1.77
L (m)	1.05×10^{-5}
$D_{e,acetic} \times 10^9$ ($m^2.s^{-1}$)	1.49
$D_{e,H_2} \times 10^8$ ($m^2.s^{-1}$)	6.24
$\eta\varphi^2{}_{acetic}$	2.56×10^{-7}
$\eta\varphi^2{}_{H_2}$	2.55×10^{-6}

3.3. Kinetic Study. This study was carried out to examine the effect of reaction variables and estimate kinetic parameters such as reaction order, rate constants and activation energy under isothermal conditions. The method of initial rate (r_0) was used to describe the kinetic data due to the complex reactions involving multiple reaction steps where secondary reactions and products of reaction may influence the rate. During the heat up phase, ≤2% conversion of acetic acid was observed under the reaction temperatures investigated. A third order polynomial regression was used to fit the concentration-time data obtained from the experimental mixture at time intervals of 40 mins for 6 h. The reaction rates were calculated by using linearized expressions of the resulting polynomial equation, and the reaction rates at time t=0 were considered as the initial reaction rates (r_0). Furthermore, the reaction order and rate constant values were calculated by plotting the log-log of initial reaction rates versus their corresponding initial concentrations (See equation 5). All

experiments were performed at a stirring speed of 1000 min^{-1} and catalyst particle size of ≤ 63 μm as established from the mass transfer analysis, to ensure the absence of internal and external mass transfer limitations. As evident from the experimental results, ethanol and ethylacetate were predominantly formed as a result of hydrogenation and esterification reactions. A detailed reaction mechanism will follow describing the reaction pathways.

3.4. Initial Concentration. The dependence of reaction rate on the concentrations of reactant species is determined by experimental observation and is described by the linearized expression of power law;

$$r = kC_A^n \quad (4)$$

$$\ln r_0 = \ln k + n \ln C_A \quad (5)$$

Figure 5 shows the concentration-time profile at different initial acetic acid concentration in the range of 0.16 – 0.5 M at 185 °C. Subsequently, rate dependence on initial acetic acid concentration was investigated at T = 185, 200 and 210 °C in the concentration range 0.16 – 0.5 M. A non-linear reaction rate dependence on initial concentration was established at different temperatures which suggest the reaction exhibited fractional order kinetics (Figure S4).[36] The reaction order from a plot of log r against log C_{AA} at 0.16 M, 0.23 M and 0.32 M was found to be 0.78, 0.86 and 0.92 respectively (Figure 6). In a similar study, Rachmady and Venice[19] reported a lower fractional order in the range of 0.2-0.4 for acetic acid hydrogenation at temperature range 147 °C– 192 °C in a fixed bed reactor.

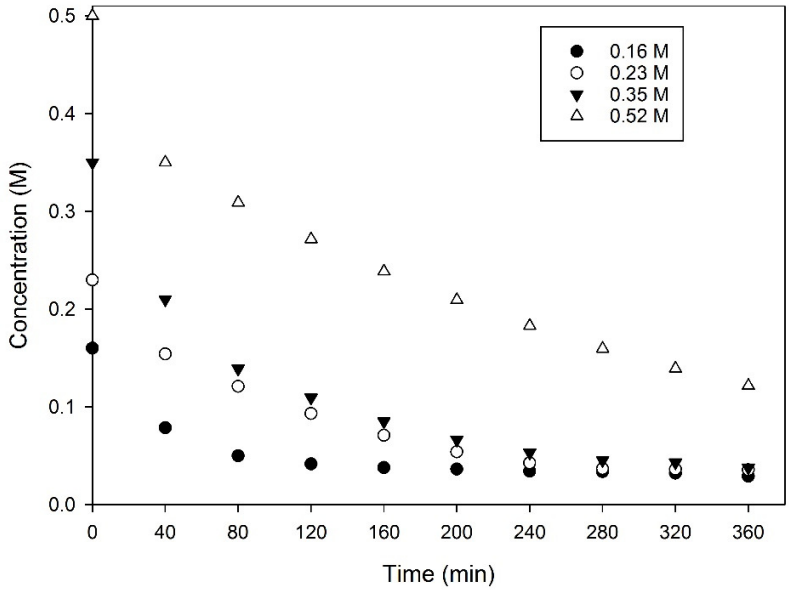

Figure 5. Concentration-Time profile at different concentration (Reaction conditions: catalyst 0.3 g, stirring speed 1000 min^{-1}, temperature 185 °C, pressure 40 bar, hexane 50 ml)

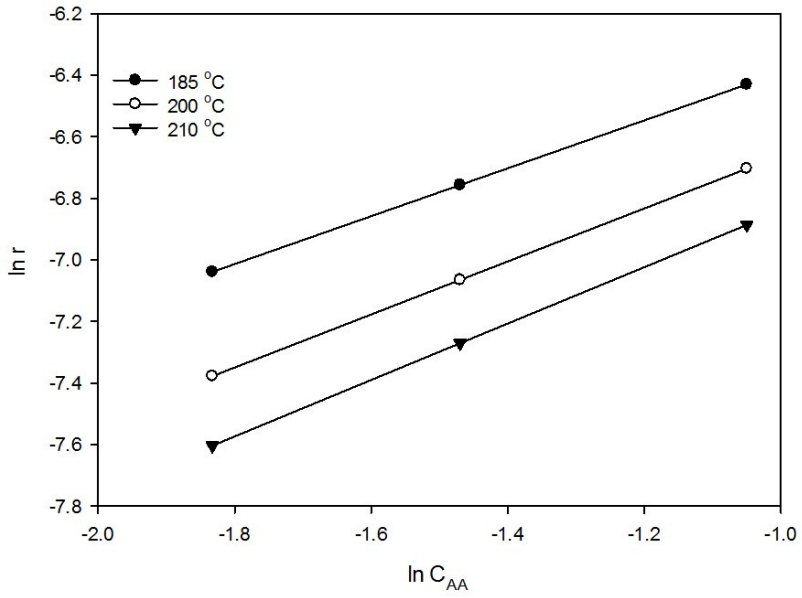

Figure 6. Plots of log r vs log C_{AA} at T = 185, 200 and 210 °C (Reaction conditions: catalyst 0.3 g, pressure 40 bar, hexane 50 ml)

3.5. Temperature. The investigation of activation energy was performed over a temperature range of 185 – 210 °C at 0.35 M of acetic acid, in order to describe temperature dependence on the reaction rate constant. Figure 7 shows the Arrhenius plot obtained from the rate constant values estimated at different temperatures from experimental data. Using the Arrhenius equation (see equation 6), the activation energy was calculated from the plot to be 48.1 kJ.mol^{-1}. A similar value has been reported in previous studies,[19,42] which is in agreement to within 4 kJ mol^{-1} obtained in this study. In contrast, Zhou et al.[18] studied hydrogenation of acetic acid using Pt-Sn catalyst supported on alumina and reported a value of 19 kJ.mol^{-1}, which might be influenced by mass transfer. Since the investigation of mass transfer in earlier section of this study confirms the absence of diffusional resistances, the experimental activation energy reported here is the true activation energy and thus the reaction can be considered to be under kinetic control.

$$lnk = ln\,A + \frac{E_A}{RT} \qquad (6)$$

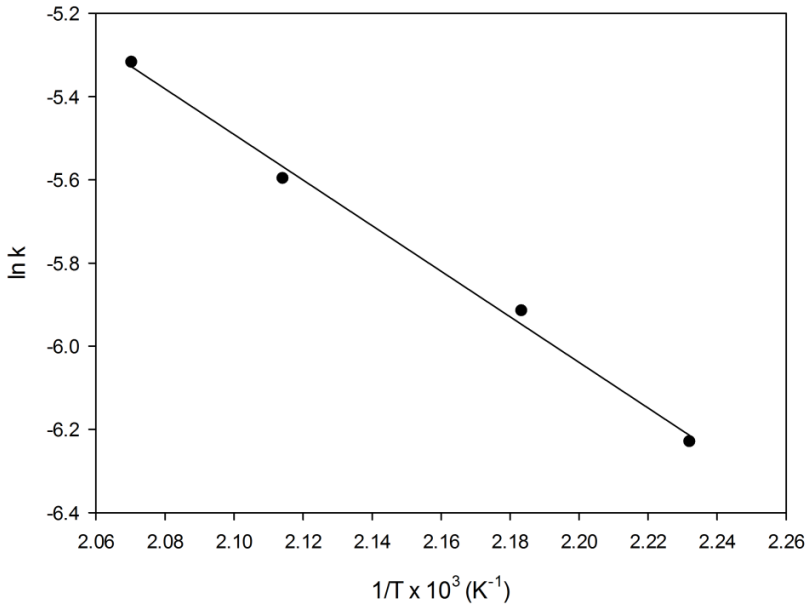

Figure 7. Arrhenius plot for activation energy of acetic acid HDO (reaction conditions: H_2 pressure, 40 bar; catalyst loading, 0.3 g; initial concentration, 0.35M; and reaction time, 6 h respectively).

3.6. Pressure. The effect of hydrogen pressure on the hydrogenation rates was studied in the range of 20-50 bar at a temperature of 200 °C and acetic acid concentration of 0.35 M as shown in Figure 8. The dependence of reaction rates on hydrogen pressure shows a non-linear trend which suggests that the reaction order with respect to hydrogen pressure is a fractional order (<1). From the log-log plot of initial rate against hydrogen pressure shown in Figure S5, the reaction order was found to be 0.41, which is characteristic of strongly adsorbed hydrogen on the catalyst surface.[36]

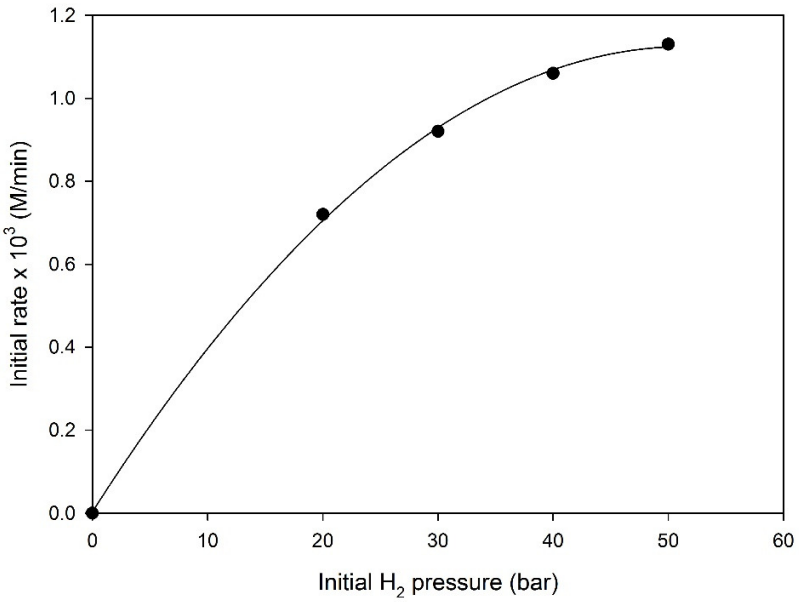

Figure 8. Pressure dependence on concentration (reaction conditions: initial concentration, 0.35 M, temperature, 185 °C; catalyst loading, 0.3 g; and reaction time, 6 h respectively).

Figure 9 shows the influence of hydrogen pressure on acetic acid conversion and the selectivity of ethanol and ethylacetate production. While acetic acid conversion increased from 75 to 93% as initial hydrogen pressure increased from 30 to 50 bar, the selectivity of ethanol increased and that of ethylacetate decreased accordingly. This observed increase in acetic acid conversion and ethanol selectivity with increased hydrogen pressure was remarkable and can be attributed to increased adsorption and dissociation of hydrogen by platinum metals. Therefore, increasing hydrogen pressure improves the hydrogenation rate of acetic acid and formation of ethanol. It can also be seen that the production of ethylacetate appears to be significant at low pressure which indicates that production of ethanol at higher pressure may be associated with increased hydrogen spill over to attack the adsorbed carbonyl group of acetic acid thereby suppressing the esterification pathway.[43] To understand the interaction of acetic acid, ethanol and ethylacetate with the catalyst surface, an adsorption study was carried out. Figure S6 shows the extent of adsorption on the surface of catalyst. It is clear that ethanol adsorbs stronger than acetic acid and ethylacetate to the catalyst, which can be summarised as thus; ethanol > acetic acid > ethylacetate. Hence, during the HDO reaction of acetic acid, the unreacted acetic acid would have been competing for active sites by reacting with formed ethanol on the catalyst surface. This shows a product inhibitory effect, explaining the higher selectivity of ethylacetate than that of ethanol at low pressure. At higher pressure, the effect of increased hydrogen spill over from the platinum sites accelerates the rate of hydrogenation which results in higher ethanol production. Several studies[19,44] have described the kinetics of hydrogenation of acetic acid and proposed that the primary products generated were acetaldehyde, ethanol and ethane via hydrogenation and HDO reactions. In contrast, this study has shown the possibility of esterification, which is a reaction between the formed ethanol and unreacted acetic acid (Figure 9).

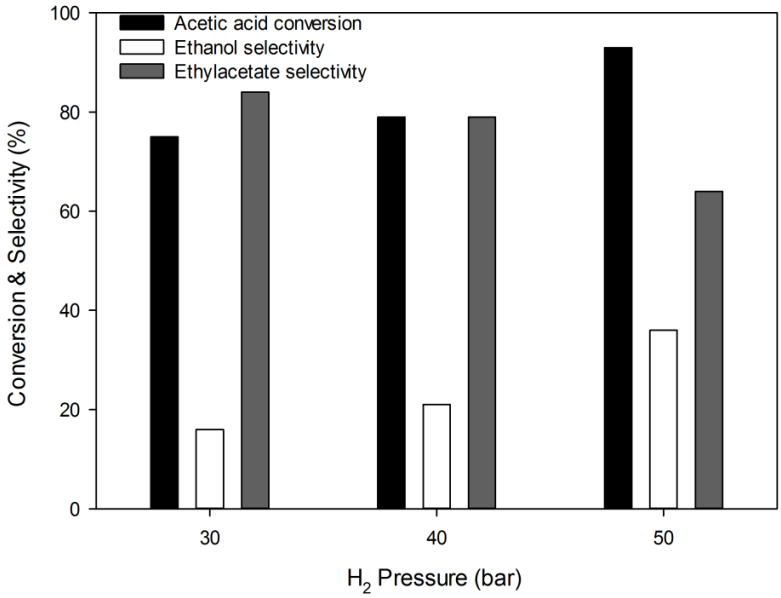

Figure 9. Effect of hydrogen pressure on product distribution (reaction conditions: initial concentration, 0.521 M, temperature, 185 °C; catalyst loading, 0.3 g; and reaction time, 2 h respectively).

3.7. Catalyst Loading. The influence of catalyst on the hydrogenation of acetic acid was studied over 4% Pt/TiO_2 in the range of 0.20 – 0.40 g catalyst loading. Figure 10 shows the influence of catalyst loading on initial reaction rate under the conditions employed during hydrogenation. The initial hydrogenation rates increased linearly with increasing catalyst loading through the origin, which further confirms the absence of gas-liquid mass transfer limitation as established from earlier section of this study. While increasing the catalyst loading affected the rate of acetic acid hydrogenation by increasing the conversion of acetic acid over the studied range of catalyst loading, selectivity to ethanol increased remarkably from 28 - 58 % while that of ethylacetate drastically decreased from 71- 41 % (Figure 11). This is expected as the esterification

is likely to be a solution phase reaction and therefore its rate is not significantly affected by the catalyst mass.

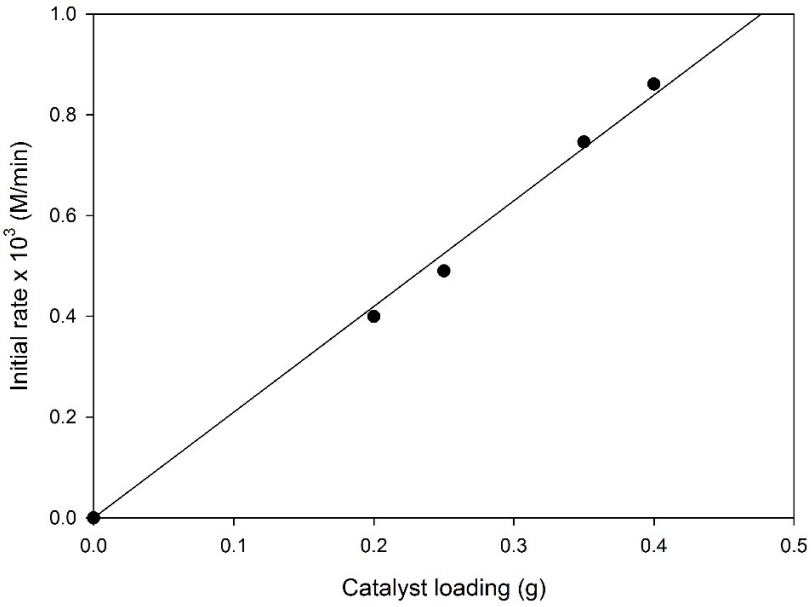

Figure 10. Effect of catalyst loading on initial hydrogenation rates (reaction conditions: initial concentration, 0.350 M, temperature, 185 °C; and H_2 pressure, 40 bar respectively).

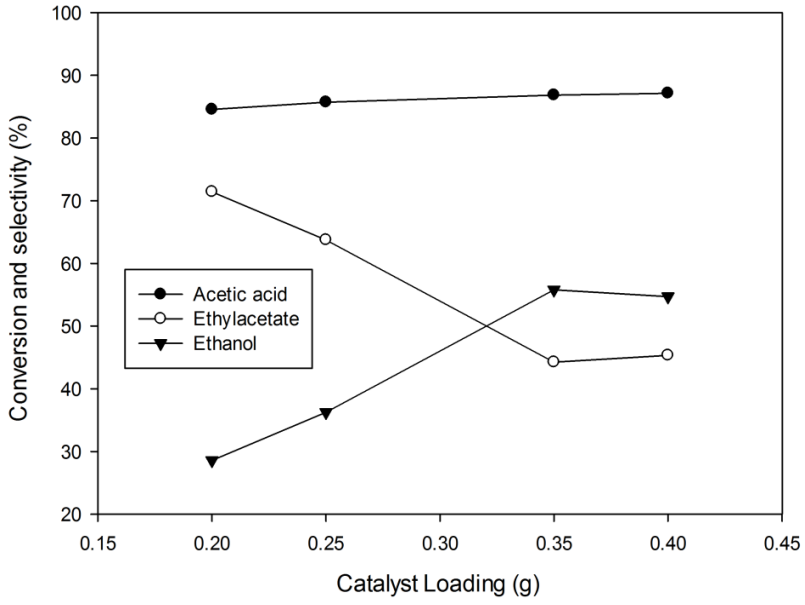

Figure 11. Effect of catalyst loading on product selectivity and acetic acid conversion after 6 h.

3.8. Reaction Mechanism and Kinetic Modelling. In this study, Langmuir-Hinshelwood-Hougen-Watson (LHHW) models were used to describe and model the initial rates of acetic acid hydrogenation based on the mechanistic steps presented by Equations 5-13. Others studies have proposed that the reaction mechanism for acetic acid hydrogenation follows adsorption of acetic acid on the support surface to generate acetyl species which are subsequently hydrogenated to form acetaldehyde and then ethanol.[45,46] In this study, the production of acetaldehyde was not apparent from the hydrogenation reaction which suggests that acetyl species reacted extremely fast as free radicals with adsorbed hydrogen species to form ethanol.[18] This was further confirmed under GC-MS analysis. The two major products were ethanol as the sole hydrogenation product and ethylacetate as a secondary product. The significant amount of ethylacetate suggests that the esterification reaction reduced the selectivity to ethanol through its subsequent reaction with hydrogenation and esterification being consecutive reaction pathways over the catalyst. This is because both reaction paths are consecutive and simultaneous reactions. A catalyst reusability test was carried out to distinguish kinetics from deactivation before interpreting and modelling the kinetic data from batch experiments as reported in our previous work.[22] A clear evolution of catalyst activity as a function of time upon reuse over three cycles indicates that the reaction rates were not influenced by catalyst deactivation.

Equations 5 and 6 show the two main reaction observed in this study. Several models have been reported for different mechanisms involving hydrogenation reactions.[29,31] A model assuming a non-dissociative adsorption of hydrogen was evaluated and was found not to be good as expected (Table S2, Table S3 and Figure S7). Therefore, a model assuming dissociative adsorption of hydrogen was considered (equation 11). The mechanism and kinetic model was only developed

for hydrogenation reaction based on equations 7, 9 and 10, since only initial reaction rate experimental data was used. In addition, the fitted model is actually a simplification of the model obtained from the mechanism, without considering ethanol adsorption term in the summation of the denominator. This term cannot be fitted using the initial reaction rate experiments because at time t=0, the concentration of ethanol is 0. Thus, the K term represents an apparent constant for the adsorption equilibrium, which is defined differently for other models where hydrogen adsorption is non-dissociative.

Hydrogenation reaction: $CH_3COOH + 2H_2 \rightarrow C_2H_5OH + H_2O$ (7)

Esterification reaction: $CH_3COOH + C_2H_5OH \rightarrow CH_3COOC_2H_5 + H_2O$ (8)

$H_{2_{(g)}} + 2^* \overset{K_H}{\leftrightarrow} 2H^*$ (9)

The surface reaction is represented as

$2H^* + CH_3COOH^{**} \overset{k}{\leftrightarrow} C_2H_5OH$ (10)

where ethanol is the main product.

Kinetic model: Competitive adsorption, dissociatively adsorbed H_2;

$$r = \frac{kC_{AA}C_{H_2}^{1/2}}{\left(1+K_{AA}C_{AA}+K_{H_2}C_{H_2}^{1/2}\right)^2} \quad (11)$$

The surface reaction is considered to be the rate-determining step as represented in equation 10.

The kinetic model was evaluated by using the Excel solver optimization program, minimum values of residual sum of squares (RSS) and coefficient of determination (R^2). The values of RSS were minimized as defined by equation 12 where r^{EXP} and r^{CAL} are the experimental and calculated reaction rates respectively.[29,31]

$$RSS = \sum_i \left(r_{exp} - r_{cal}\right)^2 \quad (12)$$

The model fit was considered for 21 points and the resulting correlation based on the R^2 value was calculated by using the relation

$$R^2 = 1 - \frac{RSS}{\sum\left(r^{EXP} - r^{MEAN}\right)^2} \quad (13)$$

where r^{MEAN} is the average experimental rates obtained from data analysis. The applicability of the model depends on the significance of R^2 value. Models with negative estimated parameters were considered thermodynamically inconsistent and thus rejected.

Table 3. Values of estimated parameters for kinetic modelling

T (°C)	k (kmol/(kgcatmin))	K_{H_2} (m^3/kmol)	K_{AA} (m^3/kmol)	Variance	RSS	R^2
185	1.7 ± 0.02	0.80 ± 0.01	3.94 ± 0.01	5.57×10^{-7}	1.66×10^{-8}	0.970
200	3.7 ± 0.01	0.53 ± 0.06	2.40 ± 0.01	1.19×10^{-7}	3.26×10^{-9}	0.973
210	5.0 ± 0.02	0.21 ± 0.03	1.50 ± 0.01	4.44×10^{-7}	3.35×10^{-9}	0.992

Table 3 presents the calculated parameters for adsorption constants, rate constants, RSS, variance and R^2 for the kinetic model. The model adequately described the kinetic data based on the estimated parameters and R^2 values which indicates there is a good agreement between the experimental and predicted rates. Further investigation of temperature dependence on the equilibrium constant and reaction rate constant was carried out using the Van't Hoff expression as shown in equation 14.

$$\ln K_{ads} = \left(\frac{-\Delta H_{ads}}{RT}\right) + \left(\frac{\Delta S}{R}\right) \quad (14)$$

where $-\Delta H_{ads}$ is the enthalpy of adsorption, ΔS is the entropy for the molecules, K_{ads} is equilibrium constant, R is gas constant and T is temperature. From Table 4, the entropy values for the molecules were negative for the model results which suggest that the reaction is

thermodynamically consistent and feasible for adsorption to occur.[19,47] The estimated activation energy based on the predicted rate constants was found to be 80.6 kJ/mol. Thus, the model seemed significant from the significant R^2 values and high activation energy.

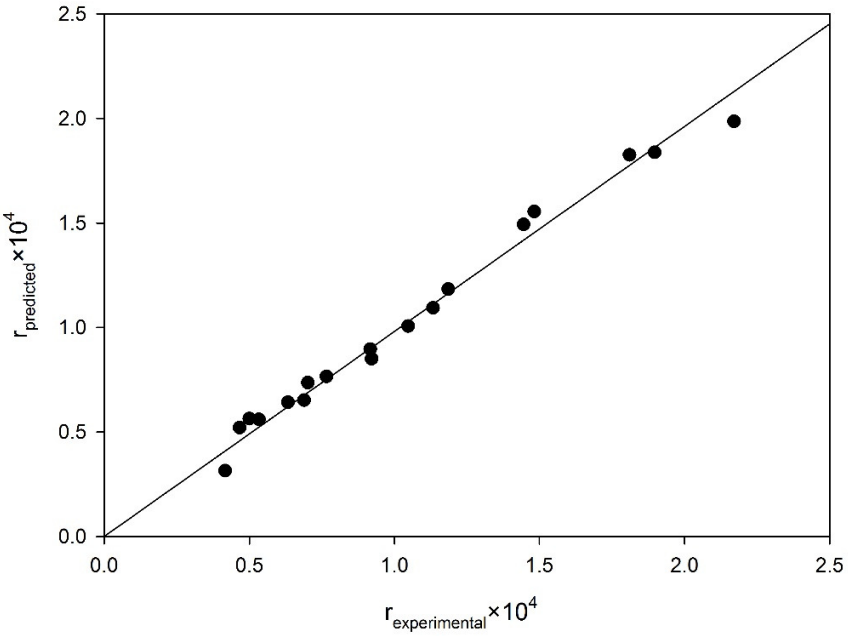

Figure 12. Parity plot for kinetic model (r^2 = 0.986)

Table 4. Values of Activation Energy and Heats of Adsorption

Parameter	**Value**	**Temperature dependence**
A_1 (kmol.kg_{cat}^{-1}.min^{-1})	4.6×10^8	$k = 4.6 \times 10^8 exp\left(\frac{-9.70}{T}\right)$
E_{act} (kJ.mol^{-1})	80.6	
A_2 (m^3.$kmol^{-1}$)	3.99×10^{-8}	$K_{AA} = 3.99 \times 10^{-8} exp\left(\frac{8.44}{T}\right)$
ΔH_{AA} (kJ.mol^{-1})	-70.20	
ΔS (kJ.$mol^{-1}K^{-1}$)	-0.142	

CONCLUSIONS

In this study, the reaction kinetics of acetic acid hydrogenation in a 100 mL batch reactor using 4% Pt/TiO_2 catalyst were investigated. The investigated reaction conditions are in the following ranges temperature (185-210 °C), initial concentration (0.16-521 M), initial H_2 pressure (20-50 bar) and catalyst loading (0.20-0.40 g) at which the system belongs to the kinetically controlled regime. A concentration dependence on reaction rate was found to be non-linear with a fractional order of 0.7-0.85. The catalytic hydrogenation of acetic acid follows consecutive reactions which results in the formation of ethanol and ethylacetate via hydrogenation and esterification reaction, respectively with no gas phase products detected. The experimental activation energy was found to be 48.1 $kJ.mol^{-1}$ for the catalytic hydrogenation of acetic acid. It was found that model and the experimental data for the modelare positively correlated with $R^2 \geq 0.97$ for all temperatures investigated. The model seemed to be feasible due to the high activation energy and dissociative adsorption of H_2.

ACKNOWLEDGEMENTS

The authors' acknowledge, with thanks, the Petroleum Technology and Development Fund (PTDF), Nigeria scholarship for Ahmed M Lawal towards this work, Dr Chi Tsang for his help with the GC method and John Wedderburn for his help with the catalyst surface area determination.

SUPPORTING INFORMATION

Materials available online include:

EDX image of 4% Pt/TiO_2.

Nitrogen adsorption-desorption isotherm for 4% Pt/TiO_2.

XRD pattern for fresh 4% Pt/TiO_2.

Concentration dependence on rate of disappearance.

Log-Log plot of initial rate against hydrogen pressure.

Adsorption study for acetic acid, ethanol and ethylacetate.

Parity Plot

Parameters used for the calculation of the minimum speed for the complete suspension of 4%Pt/TiO_2.

REFERENCES

(1) US Energy Information Administration (EIA). *Global Transportation Energy Consumption : Examination of Scenarios to 2040 using ITEDD*; 2017.

(2) Wang, H.; Male, J.; Wang, Y. Recent advances in hydrotreating of pyrolysis bio-oil and its oxygen-containing model compounds. *ACS Catal.* **2013**, *3* (5), 1047-1070.

(3) Ruddy, D. A.; Schaidle, J. A.; Ferrell, J. R., III; Wang, J.; Moens, L.; Hensley, J. E. Recent advances in heterogeneous catalysts for biooil upgrading via "ex situ catalytic fast pyrolysis": catalyst development through the study of model compounds. *Green Chem.* **2014**, *16* (2), 454– 490.

(4) Mullen, C. A.; Boateng, A. A. Chemical Composition of Bio-oils Produced by Fast Pyrolysis of Two Energy Crops. *Energy Fuels* **2008**, *22* (7), 2104-2109.

(5) Oasmaa, A.; Sipilä, K.; Solantausta, Y.; Kuoppala, E. Quality improvement of pyrolysis liquid: Effect of light volatiles on the stability of pyrolysis liquids. *Energy Fuels* **2005**, *19* (6), 2556-2561.

(6) Mortensen, P. M.; Grunwaldt, J. D.; Jensen, P. A.; Knudsen, K. G.; Jensen, A. D. A review of catalytic upgrading of bio-oil to engine fuels. Appl. Catal., A 2011, *407* (1-2), 1-19.

(7) Elliott, D. C. Historical developments in hydroprocessing bio-oils. *Energy Fuels* **2007**, *21* (3), 1792-1815.

(8) Yuan, M. L.; Xie, J. H.; Zhu, S. F.; Zhou, Q. L. Deoxygenative Hydrogenation of Amides Catalyzed by a Well-Defined Iridium Pincer Complex. *ACS Catalysis* **2016**, *6* (6), 3665–3669.

(9) Rasu, L.; John, J. M.; Stephenson, E.; Endean, R.; Kalapugama, S.; Clément, R.; Bergens, S. H. Highly Enantioselective Hydrogenation of Amides via Dynamic Kinetic Resolution Under Low Pressure and Room Temperature. *J. Am. Chem. Soc.* **2017**, *139* (8), 3065-3071.

(10) Saudan, L. A. Hydrogenation processes in the synthesis of perfumery ingredients. *Acc. Chem. Res.* **2007**, *40* (12), 1309–1319.

(11) Chakraborty, S.; Dai, H.; Bhattacharya, P.; Fairweather, N. T.; Gibson, M. S.; Krause, J. A.; Guan, H. Iron-based catalysts for the hydrogenation of esters to alcohols. *J. Am. Chem. Soc.* **2014**, *136* (22), 7869–7872.

(12) Pritchard, J.; Filonenko, G. A.; Van Putten, R.; Hensen, E. J. M.; Pidko, E. A. Heterogeneous and homogeneous catalysis for the hydrogenation of carboxylic acid derivatives: History, advances and future directions. *Chem. Soc. Rev*. **2015**, *44* (11), 3808-3833.

(13) He, D. H.; Wakasa, N.; Fuchikami, T. Hydrogenation of carboxylic acids using bimetallic catalysts consisting of group 8 to 10, and group 6 or 7 metals. *Tetrahedron Lett.* 1**995**, *36* (7), 1059–1062.

(14) Lu, Q.; Song, J.; Zhang, M.; Wei, J.; Li, C. A theoretical study on the mechanism of hydrogenation of carboxylic acids catalyzed by the Saito catalyst. *Dalton Trans.* **2018**, *47* (7), 2460–2469.

(15) Zacher, A. H.; Olarte, M. V.; Santosa, D. M.; Elliott, D. S.; Jones, S. B. A review and perspective of recent bio-oil hydrotreating research. *Green Chem*. **2014**, *16* (2), 491–515.

(16) Manyar, H. G.; Paun, C.; Pilus, R.; Rooney, D. W.; Thompson, J. M.; Hardacre, C. Highly selective and efficient hydrogenation of carboxylic acids to alcohols using titania supported Pt catalysts. *Chem. Commun.* **2010**, *46* (34), 6279-6281.

(17) Ullrich, J.; Breit, B. Selective Hydrogenation of Carboxylic Acids to Alcohols or Alkanes Employing a Heterogeneous Catalyst. *ACS Catal.* **2018,** *8* (2), 785-789.

(18) Zhou, M.; Zhang, H.; Ma, H.; Ying, W. Kinetic Modeling of Acetic Acid Hydrogenation to Ethanol over K-Modified PtSn Catalyst Supported on Alumina. *Ind. Eng. Chem. Res.* **2017**, *56* (31), 8833–8842.

(19) Rachmady, W.; Vannice, M. Acetic Acid Hydrogenation over Supported Platinum Catalysts. *J. Catal.* **2000**, *192* (2), 322-334.

(20) Wan, H.; Chaudhari, R. V.; Subramaniam, B. Aqueous Phase Hydrogenation of Acetic Acid and Its Promotional Effect on p -Cresol Hydrodeoxygenation. *Energy Fuels.* **2013**, *27* (1), 487-493.

(21) Chen, Y.; Miller, D. J.; Jackson, J. E. Kinetics of Aqueous-Phase Hydrogenation of Organic Acids and Their Mixtures over Carbon Supported Ruthenium Catalyst. *Ind. Eng. Chem. Res.* **2007**, *46* (10), 3334–3340.

(22) Lawal, A. M.; Hart, A.; Daly, H.; Hardacre, C.; Wood, J. Catalytic Hydrogenation of Short Chain Carboxylic Acids Typical of Model Compound Found in Bio-Oils. *Ind. Eng. Chem. Res.* **2019**, DOI: 10.1021/acs.iecr.9b01093.

(23) Sing, K. S. W.; Everett, D. H.; Haul, R. A. W.; Moscou, L.; Pierotti, R. A. Reporting Physisorption Data For Gas/Solid Systems. *Pure Appl. Chem.* **1985**, *57* (4), 603–619.

(24) Li, Y.; Zhang, W.; Zhang, L.; Yang, Q.; Wei, Z.; Feng, Z.; Li, C. Direct Synthesis of Al−SBA-15 Mesoporous Materials via Hydrolysis-Controlled Approach. *J. Phys. Chem. B* **2004**, *108* (28), 9739–9744.

(25) He, Z.; Wang, X. Highly selective catalytic hydrodeoxygenation of guaiacol to cyclohexane

over Pt/TiO_2 and $NiMo/Al_2O_3$catalysts. *Front.Chem.Sci.Eng.* **2014**, *8* (3), 369–377.

(26) Zhang, C.; He, H.; Tanaka, K. Catalytic performance and mechanism of a Pt/TiO_2 catalyst for the oxidation of formaldehyde at room temperature. *Appl. Catal., B* **2006**, *65* (1-2), 37-43.

(27) Zhang, Z.; Jackson, J. E.; Miller, D. J. Kinetics of Aqueous-Phase Hydrogenation of Lactic Acid to Propylene Glycol. *Ind. Eng. Chem. Res.* **2002**, *41* (4), 691–696.

(28) Bindwal, A. B.; Vaidya, P. D. Reaction kinetics of vanillin hydrogenation in aqueous solutions using a Ru/C catalyst. *Energy Fuels* **2014**, *28* (5), 3357-3362.

(29) Jain, A. B.; Vaidya, P. D. Kinetics of aqueous-phase hydrogenation of model bio-oil compounds over a Ru/C catalyst. *Energy Fuels* **2015**, *29* (1), 361–368.

(30) Sipos, O.; Nagy, K.; Galajda, P. Kinetics and Mass Transfer in the Hydrogenation of 2-((1-benzyl-1,2,3,6-tetrahydropyridin-4-yl)methylene)-5,6-dimethoxy- -2,3-dihydroinden-1-one hydrochloride over Pt/C Catalyst. *Chem. Biochem. Eng. Q.* **2014**, *28* (2), 233–240.

(31) Bindwal, A. B.; Vaidya, P. D. Kinetics of Aqueous-Phase Hydrogenation of Levoglucosan over Ru/C Catalyst. *Ind. Eng. Chem. Res.* **2013**, *52* (50), 17781−17789.

(32) Tike, M. A.; Mahajani, V. V. Kinetics of liquid-phase hydrogenation of furfuryl alcohol to tetrahydroftirfuryl alcohol over a Ru/TiO_2 Catalyst. *Ind. Eng. Chem. Res.* **2007**, *46* (10), 3275–3282.

(33) Akpa, B. S.; D'Agostino, C.; Gladden, L. F.; Hindle, K.; Manyar, H.; McGregor, J.; Li, R.; Neurock, M.; Sinha, N.; Stitt, E. H.; Weber, D.; Zeitler, J. A.; Rooney, D. W. Solvent effects in the hydrogenation of 2-butanone. *J. Catal.* **2012**, *289*, 30–41.

(34) McManus, I.; Daly, H.; Thompson, J. M.; Connor, E.; Hardacre, C.; Wilkinson, S. K.; Sedaie Bonab, N.; Ten Dam, J.; Simmons, M. J. H.; Stitt, E. H.; D'Agostino, C.; McGregor, J.; Gladden, L. F.; Delgado, J. J. Effect of solvent on the hydrogenation of 4-phenyl-2-butanone over Pt based catalysts. *J. Catal.* **2015**, *330*, 344-353.

(35) Singh, U. K.; Vannice, M. A. Kinetics of liquid-phase hydrogenation reaction over supported metal catalysts-a review. *J. App. Catal. A* **2001**, *213* (1), 1–24.

(36) Bindwal, A. B.; Bari, A. H.; Vaidya, P. D. Kinetics of low temperature aqueous-phase hydrogenation of model bio-oil compounds. *Chem. Eng. J.* **2012**, *207–208*, 725–733.

(37) Sporka, K.; Hanika, J.; Růžička, V.; Halousek, M. Diffusion of gases in liquids. III. Diffusion coefficients of hydrogen in organic solvents. Collect. *Czech. Chem. Commun.* **2012**, *36* (6), 2130–2136.

(38) Sitaraman, R.; Ibrahim, S. H.; Kuloor, N. R. A Generalized Equation for Diffusion in Liquids. *J. Chem. Eng. Data.* **1963**, *8* (2), 198–201.

(39) Wilke, C. R; Chang, P. Correlation of diffusion coefficients in dilute solutions. *AIChE. J.* **1955**, *1* (2), 264–270.

(40) Katayama, T.; Nitta, T. Solubilities of Hydrogen and Nitrogen in Alcohols and n-Hexane *J. Chem. Eng. Data.* **1976**, *21* (2), 194–196.

(41) Brunner, E. Solubility of Hydrogen in 10 Organic Solvents at 298.15, 323.15, and 373.15 K. *J. Chem. Eng. Data.***1985**, *30* (3), 269–273.

(42) Shih, Y.-S.; Lee, C.-K. Kinetics of the Ruthenium-Catalyzed Hydrogenation of Acetic Acid to Ethanol. *J. Chin. Chem. Soc.* **1985**, *32*, 29–34.

(43) Kawamoto, H.; Tomoya, F.; Yuto, I.; Shiro, S. Effects of Different Solvents on Hydrogenation of Acetic Acid over Pt/TiO_2 for Bioethanol Production. *J. Jpn. Inst. Energy.* **2016**, *95* (2), 162-166.

(44) Liu, J.; Lyu, H.; Chen, Y.; Li, G.; Jiang, H.; Zhang, M. Insights into the mechanism of ethanol synthesis and ethyl acetate inhibition from acetic acid hydrogenation over Cu2In(100): A DFT study. *Phys. Chem. Chem. Phys.* **2017**, *19* (41), 28083-28097.

(45) Pallassana, V.; Neurock, M. Reaction paths in the hydrogenolysis of acetic acid to ethanol over Pd(111), Re(0001), and PdRe alloys. *J.Catal.* **2002**, *209* (2), 289–305.

(46) Pestman, R.; Koster, R. M.; van Duijne, A.; Pieterse, J. A. Z.; Ponec, V. Reactions of Carboxylic Acids on Oxides. *J.Catal.* **1997**, *168* (2), 265–272.

(47) Vannice, M. A.; Hyun, S. H.; Kalpakci, B.; Liauh, W. C. Entropies of adsorption in heterogeneous catalytic reactions. *J.Catal.* **1979**, *56* (3), 358–362.

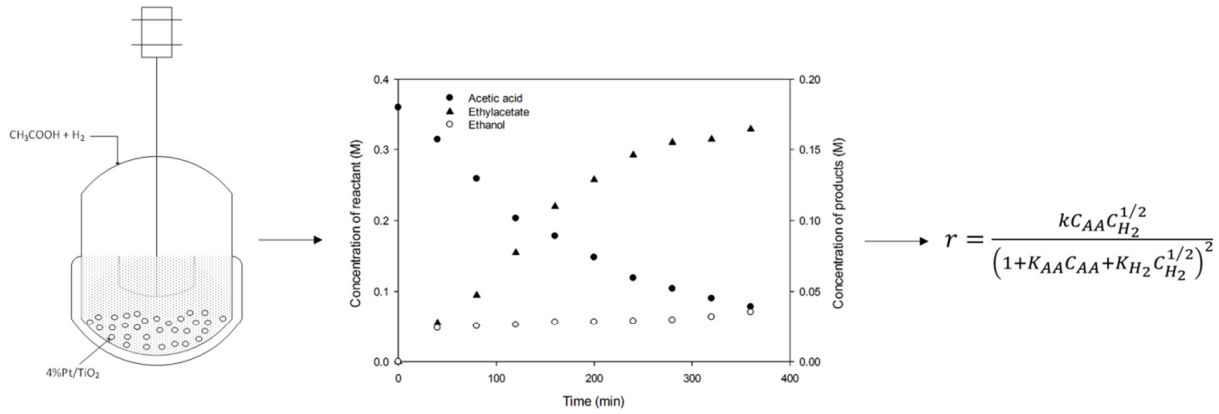

Table of contents graphic